

# Local visualization of asymmetric flux pinning by magnetic dots with perpendicular magnetization

M. J. Van Bael,\* M. Lange, S. Raedts, and V. V. Moshchalkov

*Laboratorium voor Vaste-Stoffysica en Magnetisme, K. U. Leuven, Celestijnenlaan 200D, 3001 Leuven, Belgium*

A. N. Grigorenko<sup>†</sup> and S. J. Bending

*Department of Physics, University of Bath, Claverton Down, Bath, BA2 7AY, United Kingdom*

(Received 8 May 2003; published 29 July 2003)

Field polarity-dependent flux pinning is investigated in a superconducting Pb film on an array of Co/Pt dots with out-of-plane magnetization. With the magnetic moments  $m$  of all dots aligned, the pinning force strongly depends on the mutual orientation of  $m$  and the magnetic field  $H$ . By scanning Hall probe microscopy, we have revealed the origin of this field polarity-dependent pinning. For antiparallel  $m$  and  $H$ , vortices are loosely “caged” at interstitial positions, while for parallel  $m$  and  $H$ , vortices are strongly pinned on the dots, thus providing a strong pinning asymmetry.

DOI: 10.1103/PhysRevB.68.014509

PACS number(s): 74.25.Qt, 07.79.-v, 74.25.Ha, 74.78.Db

Artificial pinning centers in superconductors are used to significantly increase the critical current density  $j_c$  and as model systems to study the fundamental properties of the interaction between flux lines and different types of pinning centers. Advances in lithography have enabled their controlled fabrication at submicron and nanometer scales.

Previous work has focused on pinning by artificial arrays of submicron holes<sup>1–8</sup> or ferromagnetic dots.<sup>9–16</sup> Matching effects between the vortex lattice and a pinning array have been observed in electrical transport and macroscopic magnetization measurements, and in molecular dynamics simulations.<sup>17,18</sup> Vortex pinning by artificial pinning arrays has also been investigated on a microscopic scale by local imaging techniques as Lorentz microscopy<sup>19</sup> and scanning Hall-probe microscopy (SHPM),<sup>13,20–24</sup> which are powerful tools for understanding the macroscopic transport and magnetization data.

When using ferromagnetic dots as pinning centers, the artificially created pinning potential in the superconducting film depends not only on the geometry, but also on the magnetic properties of the dots, such as their magnetization direction, magnetic moment, stray field direction and strength, etc. For dots with out-of-plane magnetization significantly stronger pinning was observed when the applied field  $H$  and the magnetic moments  $m$  of the dots have the same polarity (“parallel”) compared to the case of opposite polarity (“antiparallel”).<sup>10,12</sup> A local imaging study of these systems is still lacking. For the strong pinning case ( $H$  and  $m$  parallel) it is reasonable to assume that the FL’s are pinned at the dots (on-site pinning). The much weaker pinning for antiparallel  $H$  and  $m$  can result from weaker on-site pinning or from interstitial pinning where the FL’s are repelled by the dots and positioned between them due to “caging.”<sup>25</sup>

In this paper, vortex pinning is investigated in a thin Pb film with an array of submicron magnetic Co/Pt dots with perpendicular anisotropy. Macroscopic magnetization measurements reveal strongly asymmetric pinning with respect to the polarity of the applied field. We demonstrate that the interaction between FL’s and magnetic dots can be switched from attractive to repulsive by changing their mutual magnetic alignment from parallel to antiparallel. This we prove

directly via local visualization using SHPM with single vortex resolution, which provides key insights into the microscopic interaction of FL’s with magnetic pinning centers. Simple energy considerations support the SHPM observations, and reveal the microscopic origin of a pronounced field-polarity dependent pinning.

A schematic drawing of the investigated sample is given in Fig. 1. The substrate is a Si single crystal with an amorphous SiO<sub>2</sub> top layer. The magnetic dots consist of a [Co(0.3 nm)/Pt(1.1 nm)]<sub>10</sub> multilayer on a 3 nm Pt buffer layer and are fabricated by electron-beam lithography, electron-beam evaporation in ultrahigh vacuum, and lift-off techniques. They have a square shape with a side length of 400 nm and rounded corners and are arranged in a square lattice with a 1  $\mu$ m period. Hysteresis loops measured at room temperature using the magneto-optical Kerr effect have confirmed the perpendicular anisotropy of the Co/Pt dots. With  $H$  perpendicular to the substrate, the dot array had a coercive field of 2.3 kOe and showed 100% magnetic remanence. After saturating the dots  $H$  could be swept within  $-1 \text{ kOe} < H < 1 \text{ kOe}$  without changing the magnetic response of the array, indicating that the magnetic state of the dots remains virtually unchanged.

Layers of 10 nm Ge, 50 nm Pb (behaving as a type-II superconductor with critical temperature  $T_c = 7.17 \text{ K}$ ), 25 nm Ge (protective layer), and 50 nm Au were consecutively deposited on top of the dot array. The insulating Ge layers avoid proximity effects between the metallic and superconducting layers, while the Au layer facilitates the approach of the SHPM probe in a tunneling control mode. Further prepa-

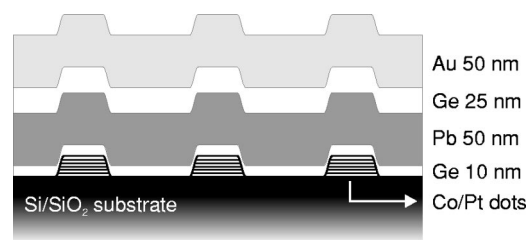


FIG. 1. Schematic drawing of a cross section of the studied sample. For clarity, vertical dimensions are  $7\times$  magnified.

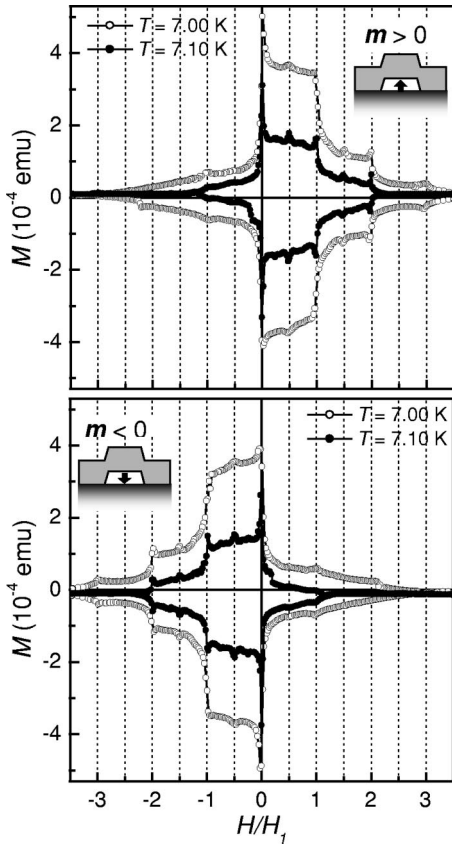


FIG. 2.  $M(H/H_1)$  magnetization curves at different temperatures near  $T_c$  (7.00 K open symbols, 7.10 K filled symbols) showing the superconducting response of the Pb layer on top of the Co/Pt dot array with all dots aligned in a positive (upper panel) and negative (lower panel) sense.  $H_1 = 20.68$  Oe is the first matching field.

ration details are given elsewhere.<sup>11–13,26</sup> The penetration depth  $\lambda(0) = 48$  nm and the coherence length  $\xi(0) = 35$  nm in our sample could be estimated from electrical transport measurements on a 25 nm reference Pb film. Close to  $T_c$ , when  $\lambda \gg t$ , with  $t = 50$  nm the thickness of the superconducting layer in our sample, this results in an effective penetration depth  $\Lambda(T) = \lambda^2(T)/t = 46$  nm/(1 -  $T/T_c$ ).

The macroscopic pinning properties of the hybrid system (dots with superconducting film) are investigated in a Quantum Design superconducting quantum interference device (SQUID) magnetometer. Figure 2 shows  $M(H)$  magnetization curves near  $T_c$  in perpendicular field  $H$  after the dots were magnetized above  $T_c$  in  $H = +40$  kOe (i.e.,  $m > 0$ ) and  $H = -40$  kOe ( $m < 0$ ) perpendicular to the surface. The field axes are normalized to the first matching field  $H_1$  given by  $\mu_0 H_1 = \phi_0/1 \mu\text{m}^2 = 2.068$  mT at which exactly one superconducting flux quantum  $\phi_0$  is generated per unit cell of the dot array. The width of the loop  $\Delta M = M^+ - M^-$  (with  $M^+$  and  $M^-$  the upper and lower branches) can be considered proportional to the critical current density  $j_c(H)$ .<sup>5</sup> When  $H$  and  $m$  have the same polarity, we observe a large width  $\Delta M(H)$  and pronounced matching effects at integer (1, 2, and 3) and several fractional multiples (1/4, 1/3, 1/2, 2/3, 3/4, 5/4, 4/3, 3/2, 5/3, and 7/4) of  $H_1$ . The matching effects indicate the presence of commensurate vortex configurations in

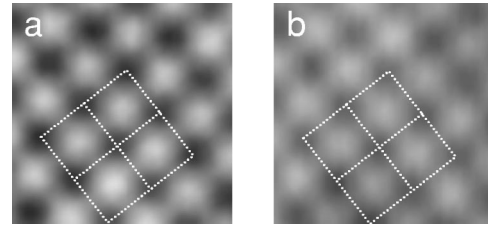


FIG. 3. Zero field SHPM images showing the local induction  $b_z$  above the sample surface over a  $(4.2 \mu\text{m})^2$  area at (a)  $T = 7.4$  K  $> T_c$  and (b)  $6.8$  K  $< T_c$  after magnetizing the dots in a negative field ( $m < 0$ ). The dots appear as dark spots, the dotted line indicates the square dot array. The peak-to-valley contrast is 0.30 and 0.25 G for (a) and (b), respectively.

a strong periodic pinning potential. If  $H$  and  $m$  have opposite polarity,  $\Delta M$  is substantially reduced and weak matching features are observed at  $|H/H_1| = 1/2$ , and 1.

High-resolution SHPM was used at low temperatures to image the local magnetic induction  $b_z(x, y)$  above the sample surface. The experimental setup is based on a modified commercial low temperature scanning tunneling microscope (STM), in which a microfabricated GaAs/AlGaAs heterojunction chip replaces the tunneling tip. The Hall cross ( $0.25 \mu\text{m}$  wire width) is defined in the 2D-electron gas at the corner of the chip a few  $\mu\text{m}$  away from an integrated STM tip. The used SHPM set-up at the University of Bath is described in more detail in Ref. 27. To increase the signal-to-noise ratio, the images shown in this paper are obtained by averaging several (typically 20) image scans.

To reveal the microscopic origin of the strong  $M(H)$  asymmetry, we have used SHPM to investigate the vortex patterns in the sample. Images are first recorded in zero applied field at temperatures slightly above and below  $T_c$ . When the dots are magnetized in a large negative perpendicular field, they appear as a square array of dark spots at  $T = 7.4$  K  $> T_c$  [Fig. 3(a)]. The peak-to-valley  $b_z$  contrast of the image in Fig. 3(a) is 0.30 G. After zero field cooling the sample to  $T = 6.8$  K  $< T_c$  the  $b_z$  peak-to-valley amplitude decreases by about 20% to 0.25 G, as can be clearly seen from the weaker contrast in Fig. 3(b). This effect is believed to be due to the response of the superconductor to the local magnetic stray field of the dots,<sup>13,15,16,23,28</sup> in which, depending on the strength of the stray field, it will be screened or non-zero fluxoids will be induced in the superconductor. Below  $T_c$  supercurrent patterns  $j_s$  appear in the Pb film encircling the dots, which depend on the amount of flux generated by a dot.<sup>15,28</sup> In our sample, the stray field of the dots is not sufficiently large to induce nonzero fluxoids in the superconductor. Consequently, local supercurrents  $j_s$  screen the flux of the dots and reduce the measured field  $b_z$  above the sample surface. The reason why the Hall probe still measures a non zero field above the dots is probably related to incomplete screening since at temperatures close to  $T_c$  the effective penetration depth is of the order of the spacing between the dots ( $\Lambda(T = 6.8 \text{ K}) \approx 900$  nm). Moreover, the field  $b_z$  is measured at a certain distance ( $\sim 200$  nm) above the superconductor surface.

Figures 4(a) and 4(b) are SHPM images obtained after

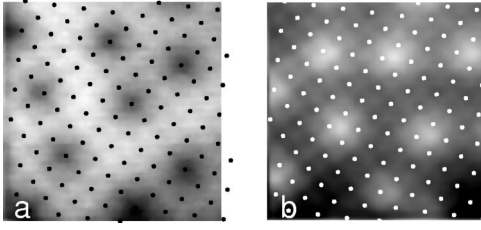


FIG. 4. SHPM images of a  $(10.5 \mu\text{m})^2$  area of the sample in  $H = -1.6$  Oe (left panel) and  $H = +1.6$  Oe (right panel), at  $T = 6.8$  K (field-cooled). The tiny black/white dots indicate the positions of the Co/Pt dots, which are all aligned in the negative sense ( $m < 0$ ). The flux lines emerge as diffuse dark ( $H < 0$ ) or bright ( $H > 0$ ) spots in the SHPM images.

field cooling the sample in small negative ( $H = -1.6$  Oe) and positive fields ( $H = +1.6$  Oe), respectively, corresponding to about 8.5 flux quanta in the scanned area of  $(10.5 \mu\text{m})^2$ . One can clearly recognize nine negative (dark) vortices in Figs. 4(a) and 8 positive (bright) vortices in Fig. 4(b), in perfect agreement with the expected number of flux quanta. The square array of dots ( $m < 0$ ) produces a much weaker contrast and is indicated by small dots for clarity. The location of the vortices depends on the field polarity. When the magnetic field of the vortex points in the same direction as the magnetic moments of the dots [Fig. 4(a),  $m < 0$  and  $H < 0$ ], the vortices are positioned at the dot sites. In contrast, vortices with opposite field polarity [Fig. 4(b),  $m < 0$ ,  $H > 0$ ] are located at interstitial positions.

These local visualization experiments can be correlated with the global magnetization experiments depicted in Fig. 2. When  $H$  and  $m$  are parallel, the flux lines are pinned by the dots and high critical currents and pronounced matching effects are observed. On the other hand, for the antiparallel alignment of  $H$  and  $m$ , the FL's are caged at interstices where they have a higher mobility and the pinning is substantially reduced.

The field polarity-dependent pinning can be explained by considering a balance of several mutually dependent energy terms. The relevant energy contributions describing a magnetic dot with fixed moment along the  $z$  direction interacting with a single FL can be written as  $E_{\text{kinetic}} + E_{\text{field}} + E_{\text{moment}}$ .  $E_{\text{kinetic}}$  is the kinetic energy associated with the total current in the system (screening current  $j_s$  of the dot and supercurrents  $j_v$  encircling the FL);  $E_{\text{field}}$  is related to the field energy in the superconductor ( $\sim \phi^2$ ) and the magnetostatic energy of the stray fields outside the SC;

$$E_{\text{moment}} = - \int_{\text{dot}} \vec{m}(\vec{r}) \cdot \vec{b}(\vec{r}) d\vec{r} \quad (1)$$

is the energy of the magnetic moment of the dot in the local field  $\vec{b}$  of the FL (see also Ref. 10). In addition, the geometric modulation of the Pb film (deposited on top of the dot pattern) can create a pinning contribution with attractive sites at the dot positions. This geometric pinning contribution is however not dependent on field polarity and we therefore leave it out of this discussion. We also do not take into ac-

count the rather small energy contributions related to the reduced order parameter in the vortex core and near the magnetic dots.

Since in our case the stray field (flux) of the dot is screened,  $E_{\text{field}}$  is effectively reduced to the field energy of the FL. Hence we need only consider  $E_{\text{kinetic}} + E_{\text{moment}}$  for on-site and interstitial pinning ( $E_{\text{kinetic}}^{\text{on-site}}$  and  $E_{\text{kinetic}}^{\text{interst}}$ ) for the case where  $H$  (or  $b_z$ ) and  $m$  are parallel and antiparallel. For the parallel case the screening currents  $j_s$  of the dot and the current  $j_v$  of the FL have opposite circulation sense and will partially cancel one another if the FL is positioned on the dot. Therefore  $E_{\text{kinetic}}^{\text{on-site}} < E_{\text{kinetic}}^{\text{interst}}$ . When  $m$  and  $b_z$  are parallel,  $E_{\text{moment}} \leq 0$ , but the energy reduction is much higher for the on-site pinning, therefore  $E_{\text{moment}}^{\text{on-site}} < E_{\text{moment}}^{\text{interst}}$ . As a result  $E_{\text{on-site}} < E_{\text{interst}}$  and the FLs are strongly pinned at the dots when  $H$  and  $m$  are parallel.

For the antiparallel alignment of  $m$  and  $H$ ,  $j_s$  and  $j_v$  have the same circulation sense. Therefore,  $E_{\text{kinetic}}^{\text{on-site}}$  is proportional to  $(j_s + j_v)^2$ . For an interstitial FL,  $E_{\text{kinetic}}^{\text{interst}}$  is roughly proportional to  $j_s^2 + j_v^2$  (assuming no overlap of the current patterns), so that  $E_{\text{kinetic}}^{\text{on-site}} \geq E_{\text{kinetic}}^{\text{interst}}$ . For the antiparallel alignment of  $m$  and  $b_z$ ,  $E_{\text{moment}}$  is always positive and  $E_{\text{moment}}^{\text{on-site}} > E_{\text{moment}}^{\text{interst}}$ . We can therefore conclude for the case of antiparallel  $m$  and  $H$  that FL's are caged interstitially, leading to much weaker pinning.

With increasing vortex density, collective effects set in due to the growing vortex-vortex interaction. For the case of parallel alignment, this leads to the observation of nicely ordered on-site pinned vortex configurations in the SHPM images at the matching fields and at fractional matching fields (e.g.,  $1/3$ ,  $1/2$ ), while the ordering of the interstitial FL's for the antiparallel case is much less pronounced due to the weak and much less confined caging. Since these collective effects do not depend on field polarity, they have no direct implication on the above discussed energy balance. Field polarity-dependent pinning has also been observed in a superconductor with in-plane oriented magnetic dipoles.<sup>13</sup> In that particular case, nonzero fluxoids were induced in the superconductor by the flux of the dipoles. Similar energy considerations with the relevant contributions in that case being  $E_{\text{field}} + E_{\text{kinetic}}$  (for in-plane dipoles,  $E_{\text{moment}}$  can be omitted) lead to the conclusion that positive flux lines would be located at the negative pole (and vice versa), in agreement with the direct SHPM observations.

In conclusion, we have investigated vortex pinning in a superconducting Pb film on an array of Co/Pt dots with perpendicular anisotropy, by combining integrated response technique (magnetization measurements) with a local probe technique (SHPM). With all dots aligned, the magnetization curve of the hybrid system is extremely asymmetric with respect to the sign of the applied magnetic field, indicating that the flux pinning strength is clearly field polarity dependent. We find strong pinning when the field and the moment of the dots point in the same direction (parallel) and much weaker pinning when they are antiparallel. Direct local studies of the pinning phenomena by SHPM and simple energy considerations yield key insights into the microscopic origin

of the field polarity-dependent pinning. The higher critical current for parallel  $m$  and  $H$  can be attributed to a stronger on-site pinning of flux lines at the dot positions. The much weaker pinning in the antiparallel case is related to the FL's caged at interstices due to the repulsive interaction with surrounding magnetic dots. This implies that for the antiparallel alignment, the unusual case of a periodic array of repulsive obstacles for the FL's is achieved, which can result in remarkable vortex dynamics (e.g., negative mobility, ratchet effect).<sup>29</sup>

The authors thank L. Van Look, K. Temst, J. Bekaert, and R. Jonckheere for help with sample preparation, J. Swerts for MOKE measurements, and Y. Bruynseraede for fruitful discussions. This work was supported by the Belgian Inter-University Attraction Poles (IUAP) and Flemish Concerted Research Actions (GOA) programs, by the ESF "VORTEX" program and by the Fund for Scientific Research-Flanders (FWO). In the U.K., this work was supported by EPSRC and MOD Grants No. GR/J03077 and GR/L96448 as well as the University of Bath Initiative Fund.

\*Electronic address: margriet.vanbael@fys.kuleuven.ac.be

†Current address: Department of Communication and Electronic Engineering, University of Plymouth, Drake Circus, Plymouth PL4 8AA, United Kingdom.

<sup>1</sup>M. Baert, V.V. Metlushko, R. Jonckheere, V.V. Moshchalkov, and Y. Bruynseraede, *Phys. Rev. Lett.* **74**, 3269 (1995).

<sup>2</sup>A.T. Fiory, A.F. Hebard, and S. Somekh, *Appl. Phys. Lett.* **32**, 73 (1978).

<sup>3</sup>A.F. Hebard, A.T. Fiory, and S. Somekh, *IEEE Trans. Magn.* **1**, 589 (1977).

<sup>4</sup>V.V. Moshchalkov, M. Baert, V.V. Metlushko, E. Rosseel, M.J. Van Bael, K. Temst, R. Jonckheere, and Y. Bruynseraede, *Phys. Rev. B* **54**, 7385 (1996).

<sup>5</sup>V.V. Moshchalkov, M. Baert, V.V. Metlushko, E. Rosseel, M.J. Van Bael, K. Temst, Y. Bruynseraede, and R. Jonckheere, *Phys. Rev. B* **57**, 3615 (1998).

<sup>6</sup>A. Castellanos, R. Wördenweber, G. Ockenfuss, A. v.d. Hart, and K. Keck, *Appl. Phys. Lett.* **71**, 962 (1997).

<sup>7</sup>M. Baert, V.V. Metlushko, E. Rosseel, V.V. Moshchalkov, and Y. Bruynseraede, *Europhys. Lett.* **29**, 157 (1995).

<sup>8</sup>V.V. Metlushko, U. Welp, G.W. Crabtree, Zhao Zhang, S.R.J. Brueck, B. Watkins, L.E. DeLong, B. Ilic, K. Chung, and P.J. Hesketh, *Phys. Rev. B* **59**, 603 (1999).

<sup>9</sup>J.I. Martín, M. Vélez, J. Nogués, and I.K. Schuller, *Phys. Rev. Lett.* **79**, 1929 (1997).

<sup>10</sup>D.J. Morgan and J.B. Ketterson, *Phys. Rev. Lett.* **80**, 3614 (1998).

<sup>11</sup>M.J. Van Bael, K. Temst, V.V. Moshchalkov, and Y. Bruynseraede, *Phys. Rev. B* **59**, 14 674 (1999).

<sup>12</sup>M.J. Van Bael, L. Van Look, K. Temst, M. Lange, J. Bekaert, U. May, G. Güntherodt, V.V. Moshchalkov, and Y. Bruynseraede, *Physica C* **332**, 12 (2000).

<sup>13</sup>M.J. Van Bael, J. Bekaert, K. Temst, L. Van Look, V.V. Moshchalkov, Y. Bruynseraede, G.D. Howells, A.N. Grigorenko, S.J. Bending, and G. Borghs, *Phys. Rev. Lett.* **86**, 155 (2001).

<sup>14</sup>Y. Jaccard, J.I. Martin, M.-C. Cyrille, M. Vélez, J.L. Vicent, and I.K. Schuller, *Phys. Rev. B* **58**, 8232 (1998).

<sup>15</sup>M.V. Milosevic, S.V. Yampolskii, and F.M. Peeters, *Phys. Rev. B* **66**, 024515 (2002).

<sup>16</sup>S. Erdin, A.F. Kayali, I.F. Lyuksyutov, and V. Pokrovsky, *Phys. Rev. B* **66**, 014414 (2002).

<sup>17</sup>C. Reichhardt, C.J. Olson, and F. Nori, *Phys. Rev. B* **57**, 7937 (1998).

<sup>18</sup>C. Reichhardt, G.T. Zimányi, R. Scalettar, A. Hoffmann, and I.K. Schuller, *Phys. Rev. B* **64**, 052503 (2001).

<sup>19</sup>K. Harada, O. Kamimura, H. Kasai, T. Matsuda, A. Tonomura, and V.V. Moshchalkov, *Science* **274**, 1167 (1996).

<sup>20</sup>S.B. Field, S.S. James, J. Barentine, V. Metlushko, G. Crabtree, H. Shtrikman, B. Ilic, and S.R.J. Brueck, *Phys. Rev. Lett.* **88**, 067003 (2002).

<sup>21</sup>A.N. Grigorenko, G.D. Howells, S.J. Bending, J. Bekaert, M.J. Van Bael, L. Van Look, V.V. Moshchalkov, Y. Bruynseraede, G. Borghs, I.I. Kaya, and R.A. Stradling, *Phys. Rev. B* **63**, 052504 (2001).

<sup>22</sup>A.N. Grigorenko, S.J. Bending, M.J. Van Bael, M. Lange, V.V. Moshchalkov, H. Fangohr, and P.A.J. de Groot, *Phys. Rev. Lett.* **90**, 237001 (2003).

<sup>23</sup>M. Lange, M.J. Van Bael, Y. Bruynseraede, and V.V. Moshchalkov, *Phys. Rev. Lett.* **90**, 197006 (2003).

<sup>24</sup>H.D. Hallen, R. Seshatri, A.M. Chang, R.E. Miller, L.N. Pfeiffer, K.W. West, C.A. Murray, and H.F. Hess, *Phys. Rev. Lett.* **71**, 3007 (1993).

<sup>25</sup>L. Radzihovsky, *Phys. Rev. Lett.* **74**, 4923 (1995).

<sup>26</sup>M. Lange, M.J. Van Bael, V.V. Moshchalkov, and Y. Bruynseraede, *Appl. Phys. Lett.* **81**, 322 (2002).

<sup>27</sup>A. Oral, S.J. Bending, and M. Henini, *Appl. Phys. Lett.* **69**, 1324 (1996).

<sup>28</sup>I.K. Marmorkos, A. Matulis, and F.M. Peeters, *Phys. Rev. B* **53**, 2677 (1996).

<sup>29</sup>C. Reichhardt and C.J. Olson Reichhardt, cond-mat/0212576 (unpublished).